Characterization of Human UDP-Glucose Dehydrogenase Reveals Critical Catalytic Roles for Lysine 220 and Aspartate 280†

Katherine E. Easley,‡ Brandi J. Sommer,‡ Gina Boanca, Joseph J. Barycki, and Melanie A. Simpson*

Department of Biochemistry, University of Nebraska, Lincoln, Nebraska 68588-0664

Received July 30, 2006; Revised Manuscript Received November 14, 2006

ABSTRACT: Human UDP-glucose dehydrogenase (UGDH) is a homohexameric enzyme that catalyzes two successive oxidations of UDP-glucose to yield UDP-glucuronic acid, an essential precursor for matrix polysaccharide and proteoglycan synthesis. We previously used crystal coordinates for *Streptococcus pyogenes* UGDH to generate a model of the human enzyme active site. In the studies reported here, we have used this model to identify three putative active site residues: lysine 220, aspartate 280, and lysine 339. Each residue was site-specifically mutagenized to evaluate its importance for catalytic activity and maintenance of hexameric quaternary structure. Alteration of lysine 220 to alanine, histidine, or arginine significantly impaired enzyme function. Assaying activity over longer time courses revealed a plateau after reduction of a single equivalent of NAD^+ in the alanine and histidine mutants, whereas turnover continued in the arginine mutant. Thus, one role of this lysine may be to stabilize anionic transition states during substrate conversion. Mutation of aspartate 280 to asparagine was also severely detrimental to catalysis. The relative position of this residue within the active site and dependence of function on acidic character point toward a critical role for aspartate 280 in activation of the substrate and the catalytic cysteine. Finally, changing lysine 339 to alanine yielded the wild-type V_{max}, but a 165-fold decrease in affinity for UDP-glucose. Interestingly, gel filtration of this substrate-binding mutant also determined it was a dimer, indicating that hexameric quaternary structure is not critical for catalysis. Collectively, this analysis has provided novel insights into the complex catalytic mechanism of UGDH.

UDP-glucuronic acid is a requisite precursor for synthesis of extracellular matrix polysaccharides, a branch point for production of additional intracellular UDP-esterified sugars, and a substrate for lipophilic xenobiotic detoxification by glucuronosyltransferase enzymes in the liver and gastrointestinal tract (*1*). UDP-glucuronic acid is generated intracellularly by UDP-glucose dehydrogenase (UGDH),[1] which catalyzes two successive NAD^+-dependent oxidations of UDP-glucose. The normal cellular functions of UGDH have been studied in various organisms by targeted gene disruptions, and these studies demonstrate its importance, particularly for developmental morphogenesis (*2*−*5*). Recently, Vigetti et al. (*6*) additionally demonstrated that the manipulation of UGDH expression levels in *Xenopus* impacts production of the extracellular glycosaminoglycan polymer, hyaluronan, which depends upon the availability of UDP-glucuronic acid. Elevated hyaluronan production is strongly implicated in cancer progression (*7*−*9*), and inhibition of hyaluronan synthesis restricts in vivo tumor growth (*10*). Therefore, limitation of UDP-glucuronic acid availability in tumor cells by UGDH antagonism may regulate the production of hyaluronan in tumors and present novel therapeutic targets. Mechanistic details of the enzyme reaction would be useful for designing rational inhibition strategies.

Bovine (*11*−*19*), streptococcal (*20*−*24*), plant (*25*, *26*), and human (*27*, *28*) UGDH enzymes have been reported, and all catalyze the same substrate to product conversion. However, the human and bovine enzymes occur as homohexamers (*16*), while the bacterial enzyme is dimeric in crystal structures (*22*) and may be active as a monomer (*20*). Studies of other nucleotide sugar dehydrogenases (*29*) have suggested that higher-order quaternary assembly influences allosteric regulation of the enzyme function but is not required for catalytic activity. An interesting feature of the enzyme mechanism as characterized in the bovine and bacterial systems is the fact that both oxidative events required to convert the 6′-hydroxyl of UDP-glucose to a carboxylate in UDP-glucuronate occur in succession at the same enzyme active site without detectable release of an intermediate (*11*, *24*; Scheme 1). Chemical reactivity of an active site lysine led investigators studying the bovine enzyme to propose that formation of a Schiff base between the 6′-carbon and the ϵ-amino group of the lysine was a plausible first step (*13*). Oxidation of the substrate as a covalent adduct would allow the enzyme to exchange NADH for NAD^+ and undergo a second round of oxidation without releasing the intermediate aldehyde. This aldimine would then be attacked by a reactive cysteine sulfhydryl which

† This work was supported by NIH Grant R01 CA106584 and NIH NCRR Grant P20 RR018759 (to M.A.S.).

* To whom correspondence should be addressed: Department of Biochemistry, University of Nebraska, N241 Beadle Center, Lincoln, NE 68588-0664. Telephone: (402) 472-9309. Fax: (402) 472-7842. E-mail: msimpson2@unl.edu.

‡ These authors contributed equally to this paper.

[1] Abbreviations: UGDH, UDP-glucose dehydrogenase; UDP, uridine 5′-diphosphate; NAD, nicotinamide adenine dinucleotide; SDS−PAGE, sodium dodecyl sulfate−polyacrylamide gel electrophoresis; IPTG, isopropyl β-D-thiogalactopyranoside; DTT, dithiothreitol; FPLC, fast performance liquid chromatography; PDB, Protein Data Bank.

10.1021/bi061537d CCC: $37.00
Published on Web 12/15/2006

Scheme 1

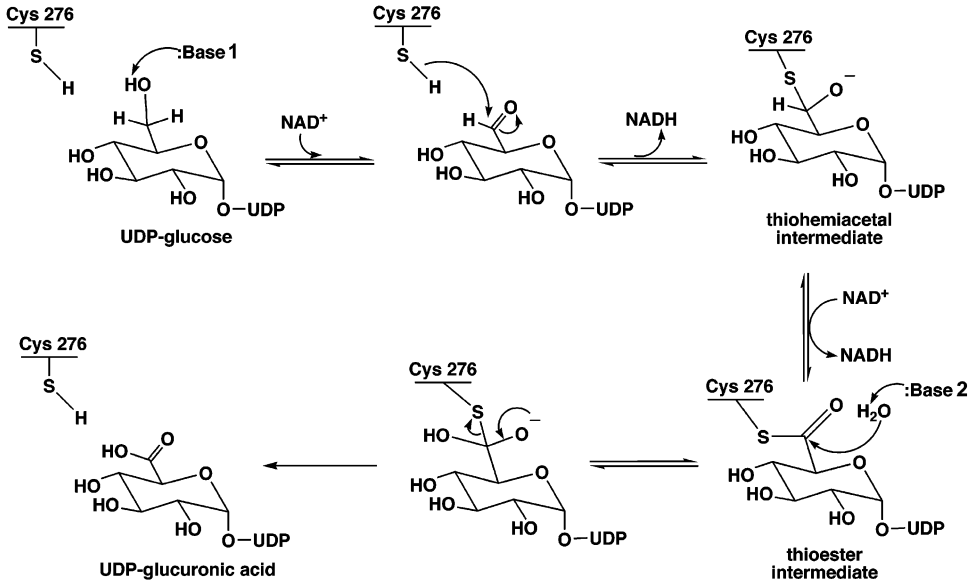

yields a thiohemiacetal that was rapidly oxidized to a thioester. Mutagenesis of cysteine to serine in the streptococcal and human enzymes has since effectively trapped the ester adduct and permitted the confirmation of this cysteine residue's catalytic function (*23*, *27*). However, the formation of a covalent lysine adduct, specifically a catalytic Schiff base, is not consistent with mechanistic aspects of the bacterial reaction (*24*). Therefore, additional molecular studies have the potential to address these questions.

Human UGDH (*28*) is 23% identical to its ortholog in *Streptococcus pyogenes*, for which a structure has been determined. Using the coordinates of the bacterial enzyme complexed with cofactor and substrate, we modeled the human enzyme and identified specific residues likely to participate in catalysis. By site-directed mutagenesis and biochemical analysis, we previously showed that the product of the first oxidation becomes linked to C276, which was important for the second oxidation. K279 was shown to be critical for both maintenance of hexameric quaternary structure and positioning of active site residues. In this work, we have generated additional mutations to characterize the catalytic function of the human enzyme. Specifically, we selected K220, K339, and D280 as critical catalytic residues, mutagenized each to assess its importance for catalysis, and further examined the function of C276. Here we describe essential roles for K220 and D280 and discuss the relationship between enzyme activity and hexameric quaternary structure.

EXPERIMENTAL PROCEDURES

Homology Modeling and Model Representation. We modeled human UGDH using 3D-PSSM (*30*), which superimposed the human amino acid sequence onto the PDB coordinates for the published *S. pyogenes* UGDH dimer (PDB entry 1DLI). A ribbon rendering of the model was made with Chimera (*31*). To facilitate selection of residues specifically involved in catalysis, the active site of a modeled ternary complex with NAD^+ and UDP-glucose was the focus as depicted in Figure 1, and proximal side chains were identified within 5 Å of the substrate and cofactor. Conservation across plant, human, bovine, murine, and bacterial species in sequence alignments of UGDH homologues was used as an additional criterion to refine our choice of appropriate putative catalytic residues. The side chains for residues examined in the study were shown colored by atom. To understand the quaternary structure influence of specific point mutations, we also modeled the dimeric unit of human UGDH against the dimeric *S. pyogenes* structure. The dimer was displayed in a ribbon representation using Chimera, with specific residues that destabilized the interfaces between trimers of dimers, as well as the substrate and cofactor, represented in space filling models (Figure 6).

Generation and Purification of UGDH Point Mutants. Point mutants of UGDH were generated from the wild-type UGDH-pET28a construct using the QuikChange site-directed mutagenesis kit (Stratagene, La Jolla, CA) according to the manufacturer's protocol. Point mutant coding sequences were subcloned in pET28a. Subclone sequences were verified by the Genomics Core at the University of Nebraska. Point mutants were expressed and purified as previously described (*27*). Briefly, the recombinant plasmids encoding N-terminal six-His fusions to UGDH and point mutants K220A, K220H, K220R, C276A, D280N, D280E, and K339A were used to transform *Escherichia coli* strain Rosetta2(DE3)pLysS (EMD Biosciences, Inc., San Diego, CA). Cultures were grown to an A_{600} of 0.6−0.8 in 2×YT medium containing 34 mg/L chloramphenicol and 30 mg/L kanamycin at 30 °C and induced for 4 h by the addition of IPTG to a final concentration of 0.5 mM. Pelleted cells were resuspended in 50 mM sodium phosphate buffer (pH 8.0) containing 0.3 M NaCl and 10 mM imidazole and lysed by sonication. Nucleic acids were removed from the soluble fraction by polyethyleneimine precipitation. Soluble point mutants were then purified by affinity chromatography using a nickel-chelating column (Novagen) according to the manufacturer's protocol and dialyzed against 0.1 M sodium phosphate (pH 7.4) and 1 mM DTT. All protein was stored at a concentration of 10 mg/mL.

Standard Enzymatic Activity Measurement and Kinetic Characterizations. For standard screening of enzymatic

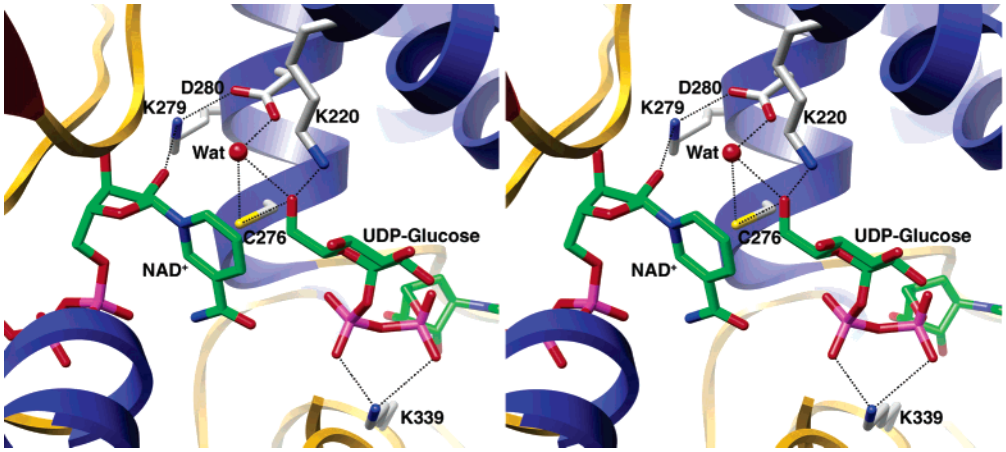

FIGURE 1: Stereodiagram of the modeled UGDH active site in a ternary complex. The human UGDH primary sequence was superimposed on the published crystal coordinates for the *S. pyogenes* enzyme (PDB entry 1DLI). A model depicting the human enzyme in complex with the NAD^+ cofactor and UDP-glucose substrate was generated using 3D-PSSM and represented in Chimera as a ribbon diagram. The active site was the focus, and side chains of specific residues discussed in the text are shown. The network of hydrogen bonding between protein active site residues and the cofactor and substrate is illustrated with dotted lines (Discussion). The overall helical ribbon is colored blue and the random coil yellow; within the active site, carbon atoms of the protein are colored gray, carbons in the cofactor and substrate are colored green, nitrogen is colored blue, oxygen is colored red, sulfur is colored yellow, and phosphorus is colored pink.

activity, the change in absorbance at 340 nm that accompanies reduction of NAD^+ to NADH was monitored as reported previously (*27*). Assays were performed for 1 min at room temperature with 10 μg of purified UGDH in 0.1 M sodium phosphate buffer (pH 7.4) containing 1 mM UDP-glucose and 10 mM NAD^+ (Sigma-Aldrich, St. Louis, MO). Specific activities were calculated from absorbance values using the molar extinction coefficient for NADH of 6220 M^{-1} cm^{-1}. The K_m and V_{max} for UDP-glucose and NAD^+ were determined independently for the D280E mutant using standard assay conditions as described above. K339A was analyzed similarly but with the following modifications. Constants for UDP-glucose as the substrate were measured by holding the NAD^+ concentration constant and varying the UDP-glucose concentration from 0 to 10 mM. Similarly, NAD^+ kinetic measurements were made by holding the UDP-glucose concentration constant and varying the NAD^+ concentration from 0 to 6 mM. Triplicate determinations were made for each concentration increment, and data were plotted with PRISM (GraphPad Software, Inc., San Diego, CA). K_m and V_{max} were calculated by fitting the data to the Michaelis−Menten equation and assuming a single binding site each for the substrate and cofactor.

Kinetic measurements for all point mutants were initially made under standard assay conditions. However, activities of C276A, D280N, and all K220 mutants were found to be negligible at the 1 min time point. Increasing (up to 5-fold excess) or decreasing (2-fold) substrate and cofactor concentrations had no effect on either the 1 min measurements or the subsequent longer time courses that were performed. To determine if residual enzymatic activity remained, mutant protein concentrations were increased 50-fold to 2 mg/mL and assays were set up with saturating cofactor and substrate concentrations (2 mM each). The absorbance at 340 nm was monitored for 100 min on a time drive that recorded values at 1 s intervals for the K220 mutants or at 2 min intervals for the C276A and D280N mutants. Activities were calculated from the absorbance values using the molar extinction coefficient for NADH and plotted versus time to illustrate differences in kinetic behaviors as shown. Linear regression analysis was used to determine rates for D280N and C276A. For the K220 mutants, the linear initial rates (i.e., data up to 1 min for K220A and up to 10 min for K220H and K220R, as shown in the inset panels of Figure 4) were replotted and analyzed by linear regression to produce specific activity.

Determination of Cofactor Binding Constants. Quenching of intrinsic tryptophan fluorescence was previously found to be a useful method of quantifying cofactor binding in a manner independent of enzyme activity, since tryptophan fluorescence diminishes in a concentration-dependent fashion with addition of NAD^+ (*27*). Each UGDH point mutant was scanned to verify maximal tryptophan excitation at 290 nm; excitation at this value was then used to confirm maximal emission at 335 nm. The intrinsic tryptophan fluorescence was monitored using these excitation and emission values in the presence of increasing NAD^+ cofactor concentrations from 0 to 1.5 mM. Dissociation constants (K_d values) were obtained for each mutant by fitting corrected fluorescence quenching to a curve with a single-exponential decay.

Molecular Weight Determination. The molecular mass of each UGDH point mutant complex was determined by gel filtration chromatography. Purified recombinant wild-type UGDH and point mutants were individually loaded on a Superdex 200 HR 10/30 column (GE Healthcare Life Sciences, Piscataway, NJ) and separated by FPLC in 50 mM $NaPO_4$ (pH 7.0) containing 150 mM NaCl, at a flow rate of 0.25 mL/min. Sizes were determined by comparison to size exclusion chromatography high-molecular weight calibration standards chromatographed under the same conditions. The standards that were used (see the inset plot of Figure 5A) were as follows: thyroglobulin (699 kDa), ferritin (416 kDa), catalase (219 kDa), aldolase (176 kDa), albumin (67 kDa), ovalbumin (47 kDa), chymotrypsinogen A (20 kDa), and RNase A (15 kDa). Resolution was sufficient to calculate molecular masses unambiguously in multiples of 57 kDa (the calculated molecular mass of monomeric His-tagged UGDH).

RESULTS

Selection and Generation of UGDH Point Mutants. The structure for human UGDH has not yet been determined,

but the human enzyme is 23% identical to its ortholog from *S. pyogenes*, for which a structure has been published (*22*). Using the coordinates of the bacterial enzyme complexed with cofactor and substrate, we modeled the human enzyme as a ternary complex with the NAD^+ cofactor and the UDP-glucose substrate and inspected the architecture of the active site (Figure 1). On the basis of this model, we identified specific residues within the active site that were likely to be important for catalytic activity. Selected residues were located unambiguously with support from primary sequence alignments of bacterial, plant, bovine, murine, and human UGDH, in which each was also 100% conserved across species (not shown). We generated point mutations at residues K220, C276, D280, and K339 to investigate their individual contributions to the enzyme mechanism. Figure 1 illustrates the positions of these residues in the active site of the human UGDH model relative to NAD^+ and UDP-glucose. On the basis of their respective positions, we expected that K220 and D280 would be critical for the catalytic activity of the enzyme, whereas K339 was predicted to be important for substrate binding. C276 was previously identified as the catalytic cysteine shown in Scheme 1 (*27*). Point mutants were each subcloned in a bacterial expression vector that encoded an N-terminal six-histidine fusion for affinity purification. The resultant constructs expressed abundant soluble recombinant UGDH in *E. coli*, and each enzyme form was purified to homogeneity by nickel affinity chromatography. Typical yields were ≈30 mg of purified protein per liter of culture for the wild type and all mutants except K220A, which was consistently ≈10 mg/L.

Kinetic Characterization of UGDH K339A. UGDH catalyzes conversion of a UDP-glucose substrate to a UDP-glucuronic acid product, concomitantly reducing two molecules of NAD^+ to NADH. To obtain kinetic constants (K_m and V_{max}) for substrate and cofactor, steady state levels of NADH are monitored by absorbance at 340 nm and converted to specific activity. The enzymatic activity of UGDH point mutants was initially assayed for 1 min with both cofactor and substrate at concentrations several-fold in excess of the saturating concentration as compared to wild-type UGDH. Only D280E (described in the following section) and K339A had detectable activity under these conditions. Measurements to determine the dependence of the reaction on cofactor concentration were taken using purified UGDH K339A incubated with increasing concentrations of NAD^+ in the presence of a saturating level of UDP-glucose substrate (Figure 2A). Similarly, the dependence of reaction kinetics on substrate was measured by increasing the UDP-glucose concentration in the presence of a saturating NAD^+ concentration (Figure 2B). Saturation kinetics were observed for both conditions. Identical reactions with the purified wild-type UGDH were analyzed simultaneously for comparison. Data were fitted to the Michaelis−Menten equation to obtain K_m and V_{max} for the reactions catalyzed by the wild-type and mutant enzymes (Table 1). Both sets of conditions yielded a similar V_{max} of ≈800−900 nmol of NADH min^{-1} (mg of enzyme)$^{-1}$ for both wild-type UGDH and K339A. However, relative to that of the wild type, the K_m for UDP-glucose was increased ≈165-fold, to 1.5 mM, and the K_m for NAD^+ was increased ∼5-fold to 2 mM for the K339A mutant. Thus, although the maximal activity is not perturbed by the K339A mutation, its relative affinities for cofactor, and particularly for substrate, are significantly reduced.

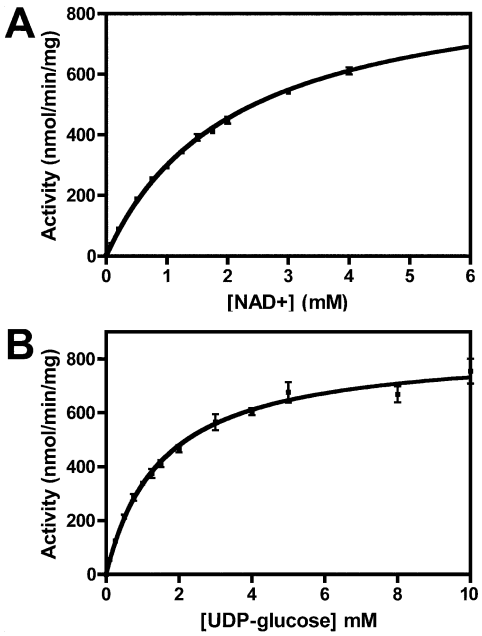

FIGURE 2: Steady state kinetics of UGDH K339A. UGDH K339A demonstrates saturable kinetics for NAD^+ (A) and UDP-glucose (B). Steady state enzyme activity was measured as the conversion of NAD^+ to NADH detected by absorbance at 340 nm. Purified human UGDH [10 μg in 0.1 M sodium phosphate (pH 7.4)] was incubated for 1 min with increasing concentrations of NAD^+ (from 0 to 6 mM) in the presence of a saturating level of substrate (UDP-glucose, 10 mM, panel A) or with increasing concentrations of UDP-glucose in the presence of a saturating level of cofactor (NAD^+, 6 mM, panel B). The specific activity was calculated from absorbance using the molar extinction coefficient for NADH and plotted as the mean ± standard deviation of three independent determinations. Data were fitted to the Michaelis−Menten equation using Prism. Constants are presented in Table 1, with concurrently measured values for the wild-type enzyme given for comparison.

Table 1: Michaelis Constants for Wild-Type, K339A, and D280E UGDH

	NAD^+		UDP-glucose	
enzyme	K_m (μM)	V_{max} (nmol min^{-1} mg^{-1})	K_m (μM)	V_{max} (nmol min^{-1} mg^{-1})
UGDH	420 ± 27	920 ± 18	9.2 ± 0.70	790 ± 15
K339A	2100 ± 75	940 ± 16	1500 ± 110	840 ± 20
D280E	530 ± 41	590 ± 15	22 ± 1.3	440 ± 12

Kinetic Characterization of UGDH C276A, D280N, and D280E Mutants. Michaelis constants for the D280E mutant were determined concurrently with those of the wild-type enzyme (Table 1). Interestingly, D280E kinetics were minimally perturbed, exhibiting a modest (≈3-fold) increase in K_m for UDP-glucose and an ≈2-fold reduced V_{max} relative to that of the wild type. To evaluate the remaining mutants more carefully and determine the extent of impaired catalytic function, we performed a time course over 100 min, measuring enzyme activity as NAD^+ turnover at 1 s intervals via the absorbance at 340 nm. Saturating substrate and cofactor concentrations were determined by increasing or decreasing the added NAD^+ and UDP-glucose concentration in 5-fold increments (not shown). Using saturating conditions, activity was plotted as a function of assay time to calculate the specific activities for the reaction (Figure 3 and Table 2). In contrast to the conversion of NAD^+ to NADH

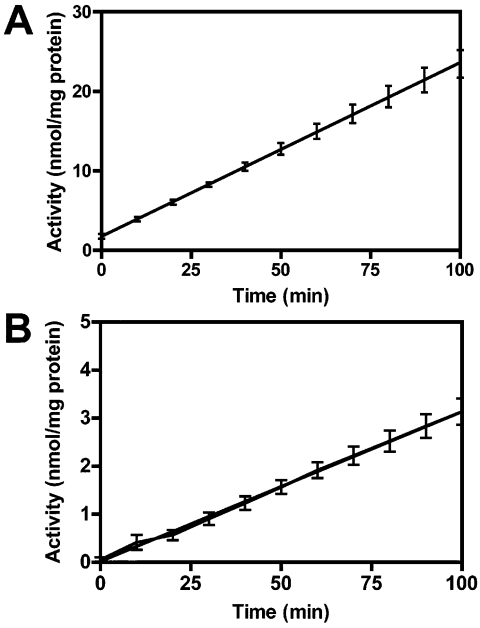

FIGURE 3: Kinetics of UGDH C276A and D280N mutants. The activity of the UGDH C276A (A) and D280N (B) mutants [2 mg/mL in 0.1 M sodium phosphate (pH 7.4)] was measured as the conversion of NAD^+ to NADH detected by absorbance at 340 nm over a 100 min time course in the presence of saturating concentrations of cofactor (2 mM NAD^+) and substrate (2 mM UDP-glucose). Absorbances were converted to specific activity using the molar extinction coefficient for NADH. Data points were collected every 2 min. Data represent the mean of three separate assays, with linear regression superimposed. The standard deviation is shown only at 10 min intervals for visual clarity.

Table 2: NAD^+ Turnover and Binding

enzyme	specific activity (nmol min^{-1} mg^{-1})	K_D (μM)
UGDH	690 ± 9.1	500 ± 12
K339A	740 ± 15	650 ± 49
K279A[a]	2.47 ± 0.11	435 ± 13
C276S[a]	2.70 ± 0.19	540 ± 16
C276A	0.220 ± 0.01	660 ± 18
D280E	410 ± 10	420 ± 5
D280N	0.031 ± 0.01	550 ± 15
K220A	2.90 ± 0.11	430 ± 12
K220H	0.400 ± 0.007	610 ± 15
K220R	0.410 ± 0.001	400 ± 9

[a] Published values from ref *27*.

by C276S, a previously characterized mutation that reached a plateau in specific activity at 1 molar equiv of NADH to added protein, cofactor reduction did not plateau during the time course of the reaction catalyzed by the C276A mutant (Figure 3A). Instead, the rate was linear and diminished approximately 3000-fold from the overall rate of NAD^+ turnover by the wild-type enzyme (Table 2). C276 is therefore important for efficient execution of the first oxidation and essential for catalysis of the second. D280N was assayed in a manner similar to that of C276A and also failed to exhibit a reaction plateau during the time course of the experiment, but specific activity was 1 order of magnitude further reduced relative to that of C276A (Figure 3B). D280 is also evidently important for both rounds of oxidation. The apparent specific requirement for acidic character suggests the low pK_a of this residue may facilitate its catalytic role. The extremely slow enzymatic turnover of both C276A and

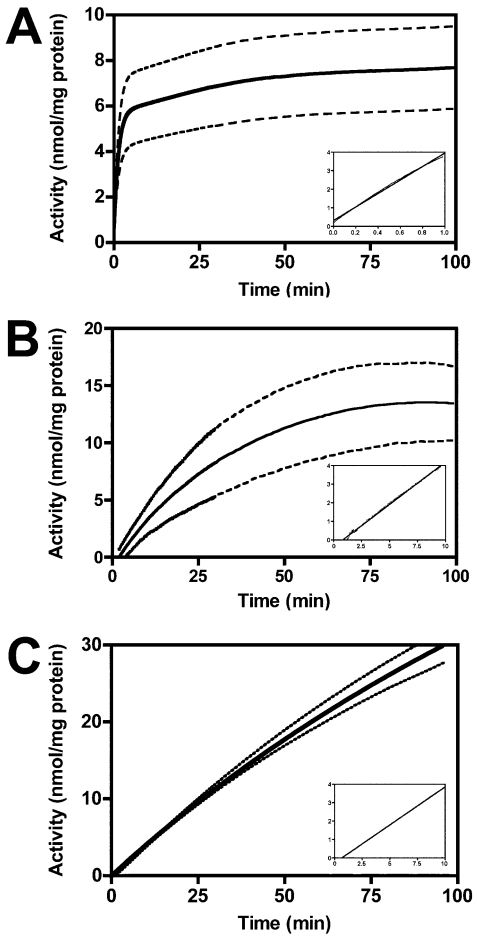

FIGURE 4: Kinetic characterization of K220A, K220H, and K220R. UGDH K220 mutants [2 mg/mL protein in 0.1 M sodium phosphate (pH 7.4)] were incubated with a saturating level of cofactor and substrate, and the absorbance was monitored at 340 nm for 100 min. Data points were collected at 1 s intervals on a time drive. Curves representing the mean of three separate determinations for each mutant are shown (thick lines). Dotted lines flanking the curves represent the standard deviation. Reactions of K220A (A) and K220H (B) reached a maximal absorbance value at molar ratios of NADH to input protein of 0.89 and 1.27, respectively, as discussed in the text. K220R (C) did not plateau during the time course of the assay. Specific activities for each mutant were obtained by linear regression analysis of the initial rates (insets). Axes for the insets are in the same units as the main axes. Note that the linear phase for K220A is on a time scale different from that for K220H and K220R.

D280N mutants precluded determination of standard K_m and V_{max} values.

UGDH K220 Mutants Exhibit Differentially Impaired Catalytic Function. The proximity of K220 to the substrate 6′-hydroxyl in the UGDH homology model suggested this residue was a likely candidate for an important catalytic role, possibly in Schiff base formation. We converted this residue to an alanine and measured its activity under saturating substrate and cofactor conditions as described for the mutants mentioned above. A relatively rapid initial increase in NADH absorbance was observed, followed by a slower phase that reached a plateau at a molar ratio of 0.89 for NADH produced versus added enzyme (Figure 4A). The K220H reaction also attained a plateau (molar ratio of 1.27 for NADH to input protein) but exhibited a slower initial rate than K220A (Figure 4B and Table 2). In contrast, K220R demonstrated linear increases in NADH production through-

out the 100 min time course (Figure 4C). Since the K220A and K220H mutants reached a maximum absorbance value for NADH production without depleting more than $^1/_{10}$ of the input NAD^+, we compared only the activity measured by the initial burst rate. Although the K220R mutant does not plateau, its activity was identical when all data were included, so it was analyzed similarly for this comparison. We excluded all but the first data points comprising the linear phase of the reaction, replotted the data with the same axes (inset graphs of Figure 4), and performed linear regression to obtain specific activities. For K220A, the initial linear phase was very rapid and the reaction was near saturation after 1 min, so only data points obtained within the first minute were used (Figure 4A, inset). For the other two mutants, data were included from the first 10 min of the reaction. Using this method, the initial rate of NADH appearance with K220A was reduced by ≈190-fold relative to a steady state rate of NADH formation by wild-type UGDH assayed with saturating substrate and cofactor levels. The activity of K220H was comparable to that of K220R but diminished relative to that of the wild-type enzyme by ≈1700-fold.

The plateau that is observed in the K220A and K220H reactions suggests that only a single round of oxidation is occurring, probably to form either the aldehyde or thiohemiacetal intermediate shown in Scheme 1. Since K220R continues to turn over and the reaction rate is dependent on the number of oxidations, activity may be used only to illustrate functional differences among the mutants. The rate-limiting step of the overall reaction determines the apparent rate for each enzyme. For the wild type, this is thioester hydrolysis, but for the mutants, an earlier step is affected by mutation and becomes rate-limiting (see the Discussion). Thus, it is appropriate only to discuss functional implications of differential activity. K220A and K220H reach an equilibrium at different rates, which could be due to increased solvent accessibility or reduced steric constraint within the active site of the former. However, neither can proceed further. K220R, although slower, may still function normally. Collectively, this suggests the positioning of a positive charge at the active site in the proximity of the site of enzymatic conversion may be important for catalysis.

Determination of UGDH Cofactor Binding Affinity. To characterize the initial binding of the NAD^+ cofactor to UGDH in a manner independent of its apparent binding during 2-fold oxidation in turnover, we monitored the UGDH intrinsic tryptophan fluorescence. We determined that the fluorescence emission of the protein at 335 nm was quenched by the incremental addition of NAD^+ (data not shown). Tryptophan quenching was plotted as a function of NAD^+ concentration and fitted to an exponential decay assuming a single binding site. The resulting dissociation constants obtained for binding by each of the point mutants were comparable (Table 2), indicating the cofactor binding domain and presumably the folded structures of the mutant proteins were unaffected by the respective point mutation. Furthermore, loss of enzymatic activity was not the result of a change in binding of NAD^+ by any mutant, and none of the residues selected were required for high-affinity cofactor binding.

Quaternary Structure of UGDH Point Mutants. Previous studies with *S. pyogenes* UGDH indicated that the enzyme

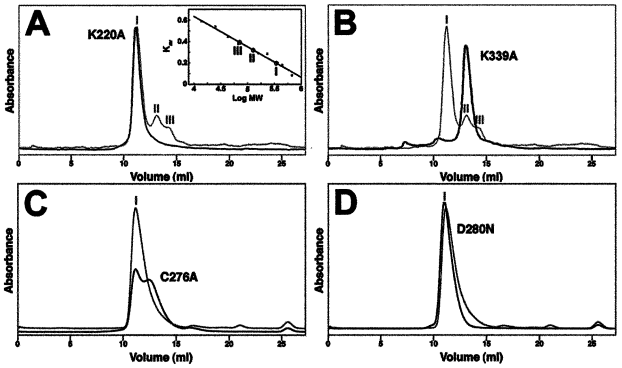

FIGURE 5: Quaternary structure of UGDH point mutants. Purified wild-type UGDH was fractionated by gel filtration FPLC on a Superdex 200 HR 10/30 resin at a flow rate of 0.25 mL/min in phosphate-buffered saline. One major and two minor peaks were detected, as discussed in the text. Size determination was made by comparison to molecular mass standards fractionated under identical conditions. The average retention time in the column was plotted vs the log of the molecular mass for each standard (inset of panel A). The following standards were used: thyroglobulin (699 kDa), ferritin (416 kDa), catalase (219 kDa), aldolase (176 kDa), albumin (67 kDa), ovalbumin (47 kDa), chymotrypsinogen A (20 kDa), and RNase A (15 kDa). Each UGDH point mutant was similarly fractionated and its molecular mass calculated from its retention time relative to the standards. The mutant quaternary structure is illustrated by superposition of FPLC traces for each point mutant (black) on the wild-type trace (gray) for comparison: (A) K220A, (B) K339A, (C) C276A, and (D) D280N.

was a dimer (*22*), but the bovine and human enzymes are considered to be hexameric (*16*, *27*). To determine the oligomeric state of human UGDH and its point mutants, we performed size exclusion analysis by FPLC (Figure 5). As we previously determined, human UGDH was predominantly observed as a hexamer, eluting from the gel filtration column at a molecular mass corresponding to 6 times the single subunit mass (peak I). Dimeric (II) and monomeric (III) species were also present in some preparations, but their appearance was independent of enzyme activity. The inset panel shows molecular weight determination for the peaks on the basis of size exclusion standards. Since the altered catalytic activity of the mutants could also result from changes in quaternary structure, the oligomeric state of the mutant enzymes was examined for perturbations relative to the wild type by size exclusion FPLC (Figure 5). K220A and D280N, although catalytically inactive or severely impaired, retain almost exclusively hexameric structure, as illustrated by an overlay of the elution profile on that of the wild-type enzyme (panels A and D of Figure 5, respectively). Similar profiles were observed for the D280E, K220H, and K220R mutants (data not shown). K339A, which had altered substrate affinity but an equivalent V_{max}, was observed to be dimeric (Figure 5B), confirming that hexameric structure is not required for the maximal activity of the wild-type human enzyme. Interestingly, whereas C276S retained a predominantly hexameric structure with a minor dimeric peak (*27*), C276A was destabilized to a hexamer−dimer mixture, with an ∼3-fold molar excess of dimer relative to hexamer.

Surface Modeling of Residues that Destabilize Quaternary Structure Suggests a Potential Orientation of Homohexamers. We constructed a model of a human UGDH dimer using the bacterial dimeric coordinates (Figure 6). There are 494 total residues in the human UGDH polypeptide, but the model depicts only amino acids 6−440, which is the stretch

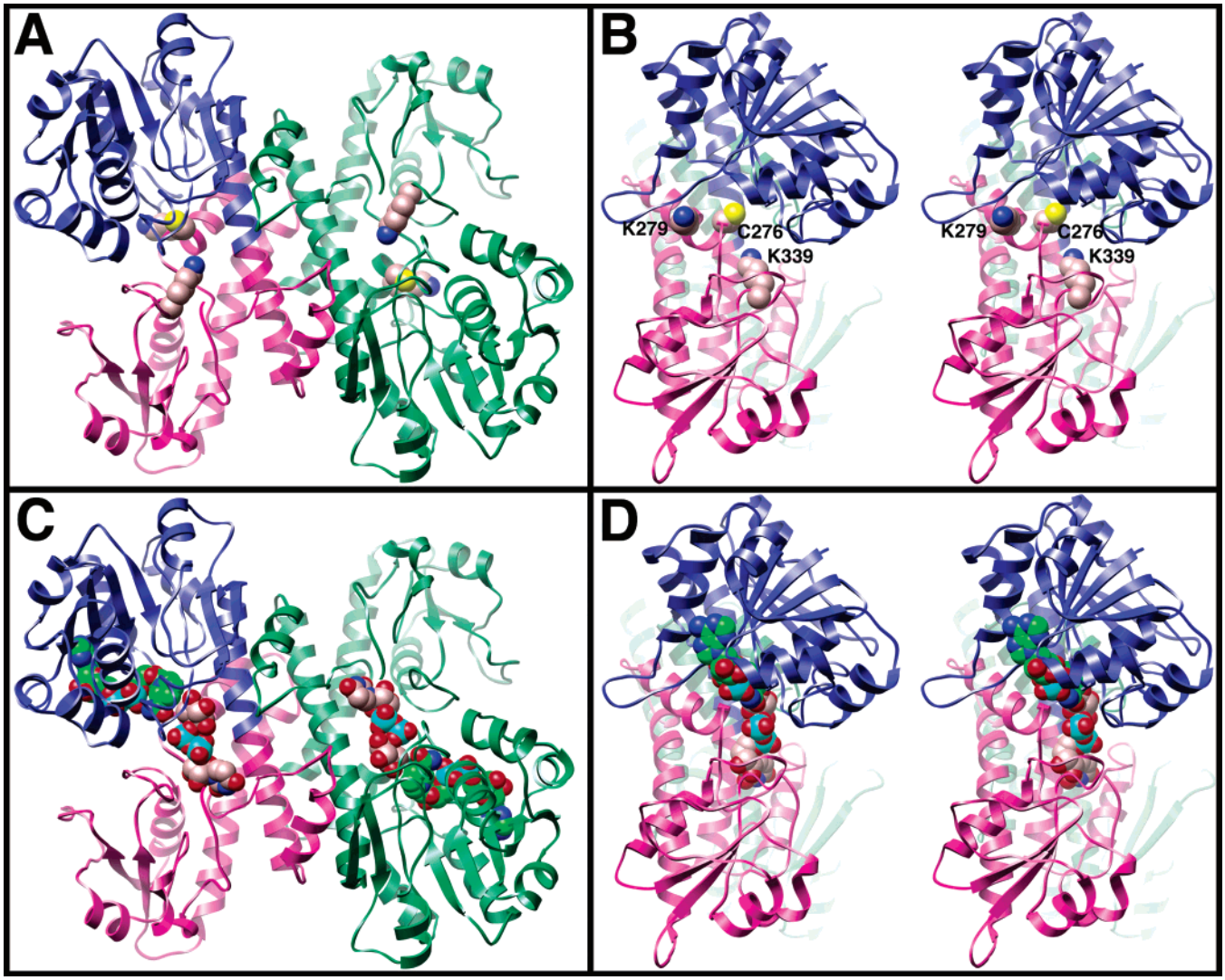

FIGURE 6: Ribbon diagram of the UGDH dimeric model. Human UGDH was modeled against the crystal coordinates for the *S. pyogenes* UGDH dimer with the NAD cofactor and UDP-glucose substrate bound. One subunit of the dimer is colored green. The other is colored blue and red-violet to illustrate the N- and C-terminal domains, respectively. The dimer is viewed from the substrate accessible face (A and C) and in stereo from the side (B and D), to illustrate the overall position of the active site, residues that are involved in maintaining quaternary structure, and the putative docking interface for association of the dimers to form a hexamer. (A and B) Side chains of K279, K339, and C276 as indicated are represented in space filling models. Carbon atoms are colored gray, and the sulfur is colored yellow and the nitrogen blue. (C and D) The cofactor and substrate are illustrated in space filling models. Carbon atoms of UDP-glucose are colored gray and those of NAD green. In both molecules, nitrogen is colored blue, oxygen red, and phosphorus cyan.

supported by homology to the bacterial enyme. Of the two modeled subunits, one monomer is colored green and the other is colored to illustrate the two globular domains that exist within each monomer. Blue is used for the N-terminal domain (residues 6−227) and red-violet for the C-terminal domain (residues 228−440). Residues we have identified to date (C276, K279, and K339) whose mutagenesis leads to the predominance of the dimeric quaternary structure are shown with space-filling representations in views from the "front" (panel A) and "side" (panel B) relative to the active site. For additional visual clarity, the side view is shown in stereo. The homology model of UGDH does not predict a surface-exposed location for K279, mutation of which was previously found to yield a dimeric enzyme, or for C276, but a partially exposed surface is modeled for K339. The relationship of these residues to the bound NAD cofactor and UDP-glucose substrate at the enzyme active site is illustrated in panels C and D of Figure 6. It is interesting to note that the majority of the enzyme's protruding features, as well as apparent routes by which cofactor, substrate, and products would enter and leave the active site, are located on the same face of the protein. This leaves the other entire face of the dimeric unit virtually flat, highlighting this surface as the probable interface for trimerization of the dimeric units. K279 may be one residue involved in direct mediation of such contacts. However, placement of the other residues suggests rather that impairment or alteration of interdomain mobility, perhaps through electrostatic contacts in the active site, in K339A and C276A mutants may destabilize the hexameric structure to favor the dimer.

DISCUSSION

Human UGDH is an enzyme required for production of UDP-glucuronic acid, a precursor for polysaccharide synthesis and chemical detoxification. Stimulation of its synthesis by androgens and peroxisome proliferators promotes its accumulation under pathological conditions, possibly contributing to a metabolic advantage for hyperproliferative

cells. In this study, we have investigated the complex catalytic mechanism of UGDH with an eye toward design of a specific inhibitor. Using previously published crystal coordinates of the streptococcal homologue, we modeled human UGDH and identified putative key active site residues. Mutagenesis of each residue allowed us to determine critical catalytic roles for K220, C276, and D280 while defining K339 as an important component of high-affinity substrate binding. Characterization of residual enzymatic activity in the catalytic mutants has afforded some new insights into the mechanism of the human enzyme.

The most straightforward mutant to evaluate is K339A, which was predicted from the model to be a substrate binding mutant. In fact, the data that were obtained support a pivotal role for K339 in providing binding energy for UDP-glucose docking. Inspection of the model reveals that K339 is ideally positioned to coordinate and screen the negative charges on the phosphate groups of this substrate. Because substrate binding is thought to precede cofactor binding in the mammalian enzyme (*12*, *32*), the reduced affinity of the K339A mutant for substrate also impacts the affinity for the NAD^+ cofactor (K_m), though its intrinsic binding (K_d) is unaffected. A similar maximum reaction velocity (V_{max}) for wild-type UGDH and K339A with respect to both substrate and cofactor demonstrates that the overall function of this mutant is not altered. Intriguingly, this mutant is exclusively found in a dimeric state, despite a clear prediction from the homology model that its location is remote from sites likely to be directly involved in maintaining "trimer of dimers" contact as has been proposed (*28*). It is not clear what role subunit associations may play in enzyme function. However, since the K339A mutant V_{max} does not differ from that of the wild-type enzyme, hexameric quaternary structure is not essential for activity. This is supported by the fact that the bacterial enzyme exists as a dimer. The overall structure of each enzyme monomer contains two distinctly folded globular domains, between which the active site exists within an extended crevice formed by association of the two domains. We postulate that in human UGDH, N-terminal and C-terminal interdomain interactions within individual monomeric subunits are essential for the maintenance of hexameric quaternary structure. K339 is the only residue to provide an active site contact from the C-terminal domain. The introduction of a hydrophobic residue at a position that is normally basic and important for substrate binding may alter interdomain movements to the extent that the hexamers are disrupted. We are currently seeking to optimize crystals of the human UGDH to test this hypothesis.

Two mechanisms have been proposed for the bovine enzyme based upon extensive kinetic data. In the first, as described in the introductory section (illustrated in Scheme 1 of refs *13* and *27*), an early step is the nucleophilic attack on the 6′-carbon to form a Schiff base intermediate that physically sequesters the substrate at the enzyme active site. The protonated Schiff base resulting from the first oxidation would then be displaced by nucleophilic attack of a cysteine sulfhydryl to produce the thiohemiacetal for the second oxidation. In support of the existence of the Schiff base, Ordman and Kirkwood (*13*) labeled a reactive lysine using a methylation method that proceeded via a Schiff base. However, the formation of a Schiff base intermediate dictates that both oxygen atoms on the 6′-carbon of the UDP-glucuronic acid product must be exchangeable with bulk solvent. Schiller et al. (*15*) performed mass spectrometric analysis of bovine UGDH reaction products formed in $H_2{}^{18}O$ and found only one of the oxygens exchanged. The finding was recently repeated by Ge and Tanner (*24*) in the bacterial system and supports an alternative mechanism in which an aldehyde intermediate is formed transiently at the active site (*20*). Since an aldehyde was not detected, the authors conclude it is rapidly converted to the thiohemiacetal adduct when it is attacked by cysteine (Scheme 1). Exchange of the first reduced cofactor for the second oxidized cofactor may occur only following thiohemiacetal formation, thus preventing release of the transient aldehyde.

Our mutagenesis studies were intended to discriminate between these alternative mechanisms in the human system. Its proximity to the C6′ hydroxyl in the enzyme active site highlighted K220 immediately as a potential candidate for catalysis. To test whether its function depended upon formation of a Schiff base, we mutagenized K220 to an alanine, thus removing its chemical and steric presence. Though the enzyme retained some activity, its initial burst phase began to saturate well below a 1:1 molar ratio of NADH per enzyme monomer. Given that the hexameric bovine complex has been shown to exhibit half-site reactivity (*16*, *19*), this point may correspond to a single oxidation within only three of the six subunits in the enzyme complex. The aldehyde species may then be slowly released from the active site, allowing the enzyme to continue performing single-turnover reactions, or it may remain bound as a thiohemiacetal, slowly exchange cofactor, and undergo a second, less favored oxidation. Formation of the thiohemiacetal and final hydrolysis may require K220. If the apparent outcome is a mixture of these equilibria, then the 0.89 molar ratio of NADH at which total saturation occurs suggests K220A can perform only single oxidations.

Possible explanations for the role of K220 that would be consistent with failure of the enzyme to continue turning over include activation of the cysteine sulfhydryl for attack on the aldehyde, stabilization of the oxyanion that forms when cysteine attacks the aldehyde to become a thiohemiacetal, and/or stabilization of the acidic carboxylate group that forms on the UDP-glucuronate product during thioester hydrolysis. Substitution of K220 with histidine was expected to preserve or enhance the potential of this residue to serve as a general acid or base during the reaction, but K220H also ceased turnover at an ~1:1 ratio of NADH to enzyme monomer. This may indicate that the role of K220 in catalytic activation does not depend on its ability to donate or abstract protons. Conversion of K220 to arginine, however, permitted sustained turnover at a slower rate, which suggests a Schiff base is not an essential catalytic species, though it does not rule out its formation. We have attempted to trap a putative Schiff base by sodium borohydride reduction using the C276S and C276A mutants but have been unsuccessful. The most obvious explanation is that K220 stabilizes oxyanionic transition states during formation of the thiohemiacetal intermediate and the carboxylate product.

The catalytic importance of C276 (C260 in *S. pyogenes* UGDH) has been established in both the human (*27*) and bacterial enzymes by site-directed mutagenesis (*23*). Conversion of this residue to serine yielded a single-turnover equilibrium that trapped the enzyme in a hemiacetal, as

confirmed by mass spectrometry (*24*). Interestingly, in both systems, substitution with alanine significantly impaired catalytic function, but the reaction did not plateau at an equimolar ratio of product to enzyme (ref *23* and this work). The C276A mutant continued to turn over slowly at a linear rate during the time course of the assay, indicating its role is not critical but facilitative. This is consistent with a model in which C276A provides an active site for UDP-glucose to undergo the first oxidation to a hexodialdose intermediate. At this point, the aldehyde can be released to allow for ongoing single turnover, or the aldehyde may remain bound at the active site, slowly hydrating while cofactor exchange occurs such that the hydrate can undergo the second oxidation. The latter explanation would account for the failure to detect the hexodialdose (*11*, *23*). Thus, the role of C276 is to drive catalysis by rapidly removing the aldehyde product of the first oxidation from the reaction equilibrium while not permitting its inefficient release and rebinding.

In addition to K220 and C276, we identified a third critical catalytic residue, D280. The contacts in the active site model (Figure 1) show that D280 and C276 are both within hydrogen bonding distance of a bound water molecule. D280 positions this water molecule at the active site, thereby indirectly linking to NAD^+, the 6′-hydroxyl of the substrate, and the C276 sulfhydryl. This water molecule may be a structural edifice, but the results obtained from analysis of the D280N and D280E mutants suggest it is an important component of the reaction mechanism. It has been postulated that the water would serve as a general base for proton abstraction during the first oxidation step in the bacterial reaction scheme (*22*). D280 may have one of several roles. (1) It may alter the pK_a of, thereby activating, a neighboring catalytic residue. (2) D280 may activate and/or ligate a tightly bound catalytic water. (3) D280 could be a general base that directly deprotonates the substrate hydroxyl. Results from our characterizations suggest that since D280N is severely but not completely impaired, its function is indirect, through activation of either the bound water or another residue. Since we have also mutagenized the other residues to which D280 is proximal and found none as impaired as the D280N mutant, we favor the activation of water as its role. The near-wild-type activity of the D280E mutant provides additional support for this scenario. When the general base carboxylate group is placed closer to C6′ of the substrate, substitution of glutamate for aspartate may obviate the requirement for a bound water to bridge the abstraction of the substrate proton. Thus, the outcome of water coordination mediated by D280 and C276 is, in effect, to convert a water molecule into a finely tuned proton donor or acceptor whose position at the active site is ideal for function.

As an overall mechanism, we propose that D280, firmly positioned by K279, which we previously showed was also important for efficient catalysis (*27*), serves to position and activate the water. The activated water may then directly abstract a proton from the C6′ hydroxyl to initiate oxidation. K220, with its unprotonated ϵ-amino group maintained by an adjacent hydrophilic residue (for example, N224 is within hydrogen bonding distance of K220), could serve to repolarize the bound water. Since C276 must be deprotonated to attack the aldehyde in the next step, the repolarized water would then activate the C276 sulfhydryl to allow thiohemiacetal formation. The positive charge on the proximal K220 amino group would stabilize the oxyanion while the second oxidation took place, and again while hydrolysis of the thioester occurred. Effective inhibition of the enzyme is likely to result from a mechanism-based covalent modification so a substrate analogue targeting C276 is an ongoing focus of research on this enzyme.

REFERENCES

1. Tukey, R. H., and Strassburg, C. P. (2000) Human UDP-glucuronosyltransferases: Metabolism, expression, and disease, *Annu. Rev. Pharmacol. Toxicol. 40*, 581−616.
2. Hacker, U., Lin, X., and Perrimon, N. (1997) The *Drosophila* sugarless gene modulates Wingless signaling and encodes an enzyme involved in polysaccharide biosynthesis, *Development 124*, 3565−3573.
3. Hwang, H. Y., and Horvitz, H. R. (2002) The *Caenorhabditis elegans* vulval morphogenesis gene sqv-4 encodes a UDP-glucose dehydrogenase that is temporally and spatially regulated, *Proc. Natl. Acad. Sci. U.S.A. 99*, 14224−14229.
4. Walsh, E. C., and Stainier, D. Y. (2001) UDP-glucose dehydrogenase required for cardiac valve formation in zebrafish, *Science 293*, 1670−1673.
5. Fraser, J. R., Laurent, T. C., and Laurent, U. B. (1997) Hyaluronan: Its nature, distribution, functions and turnover, *J. Intern. Med. 242*, 27−33.
6. Vigetti, D., Ori, M., Viola, M., Genasetti, A., Karousou, E., Rizzi, M., Pallotti, F., Nardi, I., Hascall, V. C., De Luca, G., and Passi, A. (2006) Molecular cloning and characterization of UDP-glucose dehydrogenase from the amphibian *Xenopus laevis* and its involvement in hyaluronan synthesis, *J. Biol. Chem.* (in press).
7. Auvinen, P., Tammi, R., Parkkinen, J., Tammi, M., Agren, U., Johansson, R., Hirvikoski, P., Eskelinen, M., and Kosma, V. M. (2000) Hyaluronan in peritumoral stroma and malignant cells associates with breast cancer spreading and predicts survival, *Am. J. Pathol. 156*, 529−536.
8. Ropponen, K., Tammi, M., Parkkinen, J., Eskelinen, M., Tammi, R., Lipponen, P., Agren, U., Alhava, E., and Kosma, V. M. (1998) Tumor cell-associated hyaluronan as an unfavorable prognostic factor in colorectal cancer, *Cancer Res. 58*, 342−347.
9. Aaltomaa, S., Lipponen, P., Tammi, R., Tammi, M., Viitanen, J., Kankkunen, J. P., and Kosma, V. M. (2002) Strong Stromal Hyaluronan Expression Is Associated with PSA Recurrence in Local Prostate Cancer, *Urol. Int. 69*, 266−272.
10. Simpson, M. A., Wilson, C. M., and McCarthy, J. B. (2002) Inhibition of prostate tumor cell hyaluronan synthesis impairs subcutaneous growth and vascularization in immunocompromised mice, *Am. J. Pathol. 161*, 849−857.
11. Nelsestuen, G. L., and Kirkwood, S. (1971) The mechanism of action of uridine diphosphoglucose dehydrogenase. Uridine diphosphohexodialdoses as intermediates, *J. Biol. Chem. 246*, 3824−3834.
12. Ordman, A. B., and Kirkwood, S. (1977) UDPglucose dehydrogenase. Kinetics and their mechanistic implications, *Biochim. Biophys. Acta 481*, 25−32.
13. Ordman, A. B., and Kirkwood, S. (1977) Mechanism of action of uridine diphoglucose dehydrogenase. Evidence for an essential lysine residue at the active site, *J. Biol. Chem. 252*, 1320−1326.
14. Ridley, W. P., Houchins, J. P., and Kirkwood, S. (1975) Mechanism of action of uridine diphosphoglucose dehydrogenase. Evidence for a second reversible dehydrogenation step involving an essential thiol group, *J. Biol. Chem. 250*, 8761−8767.
15. Schiller, J. G., Bowser, A. M., and Feingold, D. S. (1972) Studies on the mechanism of action of UDP-D-glucose dehydrogenase from beef liver. II. *Carbohydr. Res. 25*, 403−410.
16. Franzen, J. S., Ashcom, J., Marchetti, P., Cardamone, J. J., Jr., and Feingold, D. S. (1980) Induced versus pre-existing asymmetry models for the half-of-the-sites reactivity effect in bovine liver uridine diphosphoglucose dehydrogenase, *Biochim. Biophys. Acta 614*, 242−255.
17. Franzen, J. S., Marchetti, P. S., and Feingold, D. S. (1980) Resonance energy transfer between catalytic sites of bovine liver uridine diphosphoglucose dehydrogenase, *Biochemistry 19*, 6080−6089.
18. Franzen, J. S., Ishman, R., and Feingold, D. S. (1976) Half-of-the-sites reactivity of bovine liver uridine diphosphoglucose

dehydrogenase toward iodoacetate and iodoacetamide, *Biochemistry 15*, 5665−5671.
19. Franzen, J. S., Kuo, I., Eichler, A. J., and Feingold, D. S. (1973) UDP-glucose dehydrogenase: Substrate binding stoichiometry and affinity, *Biochem. Biophys. Res. Commun. 50*, 517−523.
20. Campbell, R. E., Sala, R. F., van de Rijn, I., and Tanner, M. E. (1997) Properties and kinetic analysis of UDP-glucose dehydrogenase from group A streptococci. Irreversible inhibition by UDP-chloroacetol, *J. Biol. Chem. 272*, 3416−3422.
21. Campbell, R. E., and Tanner, M. E. (1999) UDP-Glucose Analogues as Inhibitors and Mechanistic Probes of UDP-Glucose Dehydrogenase, *J. Org. Chem. 64*, 9487−9492.
22. Campbell, R. E., Mosimann, S. C., van De Rijn, I., Tanner, M. E., and Strynadka, N. C. (2000) The first structure of UDP-glucose dehydrogenase reveals the catalytic residues necessary for the two-fold oxidation, *Biochemistry 39*, 7012−7023.
23. Ge, X., Campbell, R. E., van De Rijn, I., and Tanner, M. E. (1998) Covalent Adduct Formation with a Mutated Enzyme: Evidence for a Thioester Intermediate in the Reaction Catalyzed by UDP-Glucose Dehydrogenase, *J. Am. Chem. Soc. 120*, 6613−6614.
24. Ge, X., Penney, L. C., van de Rijn, I., and Tanner, M. E. (2004) Active site residues and mechanism of UDP-glucose dehydrogenase, *Eur. J. Biochem. 271*, 14−22.
25. Stewart, D. C., and Copeland, L. (1998) Uridine 5′-Diphosphate-Glucose Dehydrogenase from Soybean Nodules, *Plant Physiol. 116*, 349−355.
26. Turner, W., and Botha, F. C. (2002) Purification and kinetic properties of UDP-glucose dehydrogenase from sugarcane, *Arch. Biochem. Biophys. 407*, 209−216.
27. Sommer, B. J., Barycki, J. J., and Simpson, M. A. (2004) Characterization of human UDP-glucose dehydrogenase. CYS-276 is required for the second of two successive oxidations, *J. Biol. Chem. 279*, 23590−23596.
28. Spicer, A. P., Kaback, L. A., Smith, T. J., and Seldin, M. F. (1998) Molecular cloning and characterization of the human and mouse UDP-glucose dehydrogenase genes, *J. Biol. Chem. 273*, 25117−25124.
29. Snook, C. F., Tipton, P. A., and Beamer, L. J. (2003) Crystal structure of GDP-mannose dehydrogenase: A key enzyme of alginate biosynthesis in *P. aeruginosa*, *Biochemistry 42*, 4658−4668.
30. Kelley, L. A., MacCallum, R. M., and Sternberg, M. J. (2000) Enhanced genome annotation using structural profiles in the program 3D-PSSM, *J. Mol. Biol. 299*, 499−520.
31. Huang, C. C., Couch, G. S., Pettersen, E. F., and Ferrin, T. E. (1996) Chimera: An Extensible Molecular Modeling Application Constructed Using Standard Components, *Pac. Symp. Biocomput. '96 1*, 724.
32. Franzen, J. S., Marchetti, P. S., Lockhart, A. H., and Feingold, D. S. (1983) Special effects of UDP-sugar binding to bovine liver uridine diphosphoglucose dehydrogenase, *Biochim. Biophys. Acta 746*, 146−153.

BI061537D